SQUIPABOT: a Mesoscale Parallel Robot for a Laser Phonosurgery.

Kanty Rabenorosoa, Bastien Tasca, Antonin Zerbib, Patrick Rougeot, Nicolas Andreff, Pengwang Eakkachai

SQUIPABOT: a Mesoscale Parallel Robot for a Laser Phonosurgery

Kanty Rabenorosoa*, Bastien Tasca, Antonin Zerbib,
Patrick Rougeot, and Nicolas Andreff
FEMTO-ST Institute, UMR CNRS/ENSMM/UFC/UTBM,
24 rue Alain Savary, 25000 Besancon, France
Email: name.surname@femto-st.fr

Ton Eakkachai Pengwang
Inst. of Field Robot., King Mongkut's Univ. of Technol. Thonburi,
Bangkok, Thailand
Email: eakkachai@fibo.kmutt.ac.th

April 3, 2015

Abstract

This paper presents the design of a mesoscale robot for laser phonosurgery. The proposed design is situated between conventional mechanism and MEMS technology. A combination of compliant structures and innovative micromotors enables to achieve two decoupled tilting angle, a high range (up to 45°) and a precise positioning of a laser beam. The design methodology and the optimization of the compliant structure are detailed. Preliminary results and tests are described which have induced promising performances of the mesoscale robot for laser steering.

1 INTRODUCTION

The use of laser in surgery is rapidly increasing during the past two decades. After the treatment of myopia, hypermetropia, and astigmatism [1, 2, 3], laser surgery can be used to the treatment of pathological conditions in the larynx [4, 5]. The main advantages of this

technique are its capabilities to achieve high precision microsurgeries and to improve the surgeon ergonomy. The research on endoscopic laser scalpel for vocal folds is ongoing over the world:

- FemtoLAB (Femtosecond Laser Assisted Biophotonics) from University of Texas at Austin [5, 6], where the proposed system is based on piezotube with limited scanning range but the endoscope diameter is smaller than 10mm ;
- Memorial Sloan-Kettering Cancer Center of Research Engineering Lab [4] with 17mm endoscope diameter, 2 Hz rotational velocity, but does not provide a linear control of the spot;
- the european consortium of μRALP project (`www.microralp.eu`) which develops a flexible endoscope with an actuated mirror, a stereo-vision and high speed visual servoing, and an augmented reality man-machine interface for assisted teleoperation [7].

Various challenges have been investigated including the choice of the laser type [6] and the associated optics, the development of computerized Surgeon-Machine Interface [7], the design of flexible endoscope, and the mechatronic design of microrobot to steer the high power beam. There is a difference between the beam steering for imaging systems as Optical Coherence Tomography (OCT) which is largely investigated [8, 9, 10, 11] and for laser microsurgery. Indeed a thin metal coating on thin mirror made by silicon is sufficient for imaging systems whereas the mirror can be destroyed by high power laser. In addition, the performances of the microrobot have to fit to the requirements of the vocal folds surgery. Especially, the scanning range and the accuracy of the beam positioning define the quality of the surgery. There are different techniques to steer the beam [12, 13]: tilt blocks, periscopes, Risley prisms, metastable adjustable prism, and tilt mirror. The functional requirements for beam steering system are the maximum steering angle, the resolution, the accuracy, the spot size on the impact point, the spectral range and the transmitted power.

In this paper, the mechatronic design of a mesoscale robot for laser phonosurgery is presented. It is based on an Parallel Kinematic Mechanism (PKM) orientable mirror with two decoupled tilting angles. This approach is difficult to achieve with MEMS actuator technology because it is unconvenient to transmit the electrical signals through a micro-actuator to supply another micro-actuator. The proposed concept is situated between conventional mechanism and MEMS technology due the mirror size and thickness useful to reflect an high power laser. The actuation is based on innovative piezoelectric micromotor developed by New Scale Technologies (www.newscaletech.com/), Victor, NY, USA. The proposed design aims to achieve high range tilting mirror in quasi-static conversely to MEMS mirror with limited range in static and high range in resonant frequency. In addition, a non planar mirror can be added on the platform for focusing or other beam shaping technique. In section 2, the design of Squipabot is presented. In section 3, the preliminary tests on Squipabot prototype is reported. Section 4 concludes this paper.

2 DESIGN OF SQUIPABOT

The concept presented in this paper is a mesoscale robot for high power laser steering. The robot has to be able to move a thick mirror in two tilting angles (θ_X around X axis and θ_Y around Y axis). The entire package of the robot has to be less than 8 mm x10 mm x 12 mm in order to ensure its integration in the endoscope head. The functioning principle of the steering beam robot for laser phonosurgery is shown in Fig. 2. The functional requirements of the concept are summarized in table 1 considering CO_2 or $Er:Yag$ or $Thulum$ laser.

The proposed concept is shown in Fig. 3 and is named SQUIPABOT for SQUIggle based PArallel roBOT. It can be divided in two parts: the actuator unit and the movable platform. The actuator unit is based on Squiggle piezomotors (SQL-RV-1.8) from Newscale technology which is the world's smallest linear piezo actuator. They can provide a speed about 7mm/s, a resolution about 0.5 μm, a stall force about 30 g in a volume of 2.8 mm x 2.8 mm x 6 mm.

The main advantages of this type of motor are its low voltage supply (2.3 V_{DC}), no backlash, and the blocking force without applied voltage which are specially relevant in terms of biocompatibility. According to the design and the maximum velocity of the Squiggle motor, a maximum angular velocity up to 94°/s can be achieved. The Squiggle motor are already used in some medical applications as OCT scanning [14] and laser scalpel [4, 15].

Each motor pushes the platform frames which convert the linear motion to rotation one. A preload on the motors is obtained by adding a linear spring in counter part of the platform. The steering angle α is a double of the mechanical angle $\theta_{x,y}$. Compliant joints are chosen to avoid complex assembly and backlash. The design of the movable platform is detailed in the following section.

2.1 The movable platform

The objective is to achieve two tilting angles whether ± 15° bidirectional or at least 30° unidirectional. In order to avoid a troublesome assembly and the backlashes due to conventional joint [16], compliant structures are used. In addition, the two tilting angles have to be decoupled for ensuring a simplest kinematic model and a precise control. A sketch of the movable platform is shown in Fig. 4 with two load points where to apply the equivalent force generated by the pushing motor.

The CAD model of the platform is integrated in *Comsol* Multiphysics software (see Fig. 5) for Finite Element Modeling (FEM) in order to optimize its characteristics and to study the dynamic behaviour of the platform. The effects of two parameters have been identified and studied in the following. Three undesirable displacements are identified and measured on the center of the mirror:

- the vertical displacement D_v;
- the perpendicular displacement to the rotation axis D_{pe};

- the parallel displacement to the rotation axis D_{pa}.

The objective is to minimize D_v and D_{pe} since the parallel displacement to the rotation axis does not affect the error on the screen situated at 20mm (see Fig. 2). First, let us investigate the effect of D_v and D_{pe} on the screen error. The screen is plan placed at working distance where the laser beam is observed.

2.1.1 Error on the screen

Let us calculate the error in function of D_v and D_{pe}:

$$Error = k(D_v + D_{pe} \tan \theta_{x,y}) \tag{1}$$

$$\text{where } k = \frac{\tan \theta_{x,y}(\tan(\beta + 2\theta_{x,y}) + \tan \beta)}{\tan \theta_{x,y} + \tan \beta}; \tag{2}$$

The effects of D_{pe} and D_v on the screen error were studied for different steering angles up to 45°. It can be seen in Fig. 6 that for D_v=5 μm and D_{pe}=25 μm, the error on the screen is less than 10 μm. The results are obtained with Von Mises stress (0.6 Gpa) less than the ultimate tensile strength of silicon (7 Gpa) and the applied force ($F_{z\,inner}$ and $F_{z\,outer} <$ 500μN) is less than the 0.3 N of micromotor stall force.

The design is able to fulfill the functional requirement (see Table 1) in terms of resolution. The effect of the micro-motor vibration to the resolution obtained on the screen is also investigated. It can be calculated that 1μm of vibration induces 10 μm of error on the screen for a pushing point situated at 3.3 mm from the rotation center.

2.1.2 Platform thickness

Fig. 7 shows the effect of the platform thickness T_p on the vertical displacement D_v and on the perpendicular displacement to the rotation axis D_{pe}. It is shown that D_{pe} is increasing

with the thickness of the platform. In order to minimize D_{pe} and to maintain D_v to a reasonable value, T_p is fixed about of 100 μm.

2.1.3 Spring width

The effect of the spring width on D_v and D_{pe} is also studied. It is calculated that by increasing the spring width, D_v increases too. In order to minimize the unwanted motion and to ensure a robustness of the platform, a spring width about 8 μm is chosen.

2.1.4 Dynamic behavior

For the previously defined dimensions (8 μm spring width and 100 μm platform thickness), the resonant frequency of the inner platform is 70.26 Hz and the resonant frequency of outer platform is 42.71 Hz. Angles about 1.34° and 2.20° are achievable considering the maximum velocity of the piezomotors and the resonant frequencies of the platform.

2.2 Kinematic model

A kinematic model of Squipabot with decoupled two rotations is proposed by following the modeling of parallel robot proposed by [17]. The objective is to determine the position of the the normal vector to the mirror in function of the displacement of its actuators. The robot kinematic is equivalent to four limbs parallel robot with two decoupled tilting angles are expected and the scanning angle is unidirectional with a range from 0° up to 45°.

In Fig. 9, two coordinate frames are defined: $X_BY_BZ_B$ attached to the center of fixed base and $X_PY_PZ_P$ attached to the center of moving platform. The homogenous transformation T_{BP} from the moving platform frame to the base frame is derived in Eq. 5 according to the fact that the two tilting angles are decoupled.

$$T_{BP} = R_{\theta_Y}.R_{\theta_{X/D}} \tag{3}$$

$$= \begin{bmatrix} cos\theta_Y & 0 & sin\theta_Y & 0 \\ 0 & 1 & 0 & 0 \\ -sin\theta_Y & 0 & cos\theta_Y & 0 \\ 0 & 0 & 0 & 1 \end{bmatrix} \begin{bmatrix} 1 & 0 & 0 & D_{pa} \\ 0 & cos\theta_X & sin\theta_X & D_{pe} \\ 0 & -sin\theta_X & cos\theta_X & D_v \\ 0 & & 0 & 1 \end{bmatrix} \tag{4}$$

$$= \begin{bmatrix} cos\theta_Y & sin\theta_Y sin\theta_X & cos\theta_X sin\theta_Y & D_{pa} \\ 0 & cos\theta_X & -sin\theta_X & D_{pe} \\ -sin\theta_Y & cos\theta_Y sin\theta_X & cos\theta_X cos\theta_Y & D_v \\ 0 & & 0 & 1 \end{bmatrix} \tag{5}$$

The angles θ_x and θ_y are calculated through Eq. 6.

$$\theta_x = atan(\frac{d_{m1}}{L_x});\ \theta_y = atan(\frac{d_{m2}}{L_y}) \tag{6}$$

The undesirable displacements (D_{pa}, D_{pe}, and D_v) previously listed can be integrated on the homogenous transformation to provide an accurate model. It will enable a more efficient model control based.

The contact between the platform and the motor screw is not a punctual contact due to the form of the screw head. Considering a screw head like a cap, Fig. 10 sketches the evolution of the contact and the induced angle deviation is derived in Eq. 7.

$$\delta = \arctan\frac{\Delta}{L} - \arctan\frac{\Delta - h}{L - R} \tag{7}$$

For 30° titling angle, the angle deviation is about 3.3° where $L = 3300\mu$m, Δ=1908μm, $h = 100\mu$m and $R = 550\mu$m. This angle deviation has to be taken into account to improve the accuracy of the robot in open loop control.

This section is focused on the design and a kinematic modeling of the decoupled two tilting angles. The characteristics of the movable platform were defined and its fabrication

is discussed in the following.

2.3 Fabrication

The fabrication of the movable platform is achieved on SOI (Silicon On Insulator) wafer with 100 μm of device layer, 1 μm of BOX (Burried OXide), and 400 μm of handle layer. The process flowchart is depicted in Fig. 11 where the three main etching processes are:

- Deep Reactive Ion Etching (DRIE) of the device layer (Fig. 11(a)),
- DRIE of the handle layer (Fig. 11(b)),
- etching of the BOX by Freon Reactive Ion Etching (RIE) (Fig. 11(c)) followed by Cr/Au sputtering.

A first fabrication batch was performed and the results are shown in Fig. 13.

3 PRELIMINARY TESTS

A preliminary tests were conducted to validate the concept. Squipabot is assembled (see Fig. 13) and tested on a setup composed of an external laser source, a camera, and a screen as shown on Fig. 14. A maximum steering angle up to 45° can be completed without damage. A repeating sequence was also performed to test the spring fatigue then the platform is still working after a number of tests.

3.1 Performance evaluation

The Squipabot is tested with a different trajectories (square and circle). The position of the spot is acquired by a camera and it is processed by using OpenCV (`http://opencv.org/`) and CVLink (`http://www.lab.cnrs.fr/openblockslib/cvLink.html`) libraries. An open loop control is used due to the absence of position sensor in this design. The result of path

following is shown in Fig. 16. It can be observed that the accuracy is smaller than $100\mu m$. A high level control based on fast visual servoing as presented in [18] can be implemented to improve the accuracy.

4 CONCLUSIONS

This paper presents a mesoscale robot for laser phonosurgery named Squipabot. The design proposes the combination of the conventional mechanism to MEMS technology in order to achieve a decoupled tilting angles, a high scanning range, and a precise positioning. The word's smallest piezo motor is integrated in the actuator unit of 8 mm x 10 mm x 12 mm. The use of inner and outer frame enables to decouple the two tilting angles is proposed on a movable platform made by silicon. It induces a simple kinematic model and a precise control in the future by integrating the unwanted displacements D_v and D_{pe}. The design of the movable platform is detailed and the prototype fabrication is achieved. A performance evaluation in open loop is proposed. The complete packaging of Squipabot and its integration to the flexible endoscope have been recently achieved (see 1 - c). The proposed design can be scaled down but the actuator unit has to be changed. Optimization of the spring topology in order to remove the unwanted motion and increase the robustness of the platform is ongoing. The performance improvement will be achieved by closed loop control with high speed visual servoing.

ACKNOWLEDGMENT

This work was supported by FP7 μRALP project. This work has been partially supported by the Labex ACTION project (contract "ANR-11-LABX-0001-01") and the French RENATECH network and its FEMTO-ST technological facility.

References

[1] P. D. Brazitikos, D. J. D'Amico, M.-T. Bernal, and A. W. Walsh, "Eerbium : Yag laser surgery of the vitreous and retina", *Ophthalmology* **102**, pp. 278–290 (1996).

[2] C. A. Carson and H. R. Taylor, "Excimer laser treatment for high and extreme myopia", *Archives Ophthalmology* **113**(4), pp. 431–436 (1995).

[3] SL Trokel, R Srinivasan, and B Braren, "Excimer laser surgery of the cornea", *American Journal of Ophthalmology* **96(6)**, pp. 710–715 (1983).

[4] Snehal Patel, Milind Rajadhyaksha, Stefan Kirov, Yongbiao Li, and Ricardo Toledo-Crow, "Endoscopic laser scalpel for head and neck cancer surgery", In *SPIE Vol. 8207, 82071S* (2012).

[5] C. L. Hoy, W. N. Everett, M. Yildirim, J. Kobler, S. M. Zeitels, and A. Ben-Yakar, "Towards endoscopic ultrafast laser microsurgery of vocal folds", *Journal of Biomedical Optics* **17**(3) (2012).

[6] C.L. Hoy, O. Ferhanoglu, M. Yildirim, K.H. Kim, S.S. Karajanagi, K.M.C. Chan, J. Kobler, S.M. Zeitels, and A. Ben-Yakar, "Clinical ultrafast laser surgery: recent

advances and future directions", *IEEE Journal of Selected Topics in Quantum Electronics on Nanophotonics* **20**(2), pp. 1–14 (2014).

[7] L. S. Mattos, N. Deshpande, G. Barresi, L. Guastini, and G. Peretti, "A novel computerized surgeon-machine interface for robot-assisted laser phonomicrosurgery", *The Laryngoscope* **In Press**, pp. xx (2014).

[8] K. H. Kim, B. H. Park, G. N. Maguluri, T. W. Lee, F. J. Rogomentich, M. G. Bancu, B. E. Bouma, J. F. de Boer, and J. J. Bernstein, "Two-axis magnetically-driven mems scanning catheter for endoscopic high-speed optical coherence tomography", *Optics express* **15**, pp. 18130–18140 (2007).

[9] Y. Zhu, W. Liu, K. Jia, W. Liao, and H. Xie, "A piezoelectric unimorph actuator based tip-tilt-piston micromirror with high fill factor and small tilt and lateral shift", *Sensors and Actuators A* **167**, pp. 495–501 (2011).

[10] K. Jia, S. Pal, and H. Xie, "An electrothermal tip-tilt-piston micromirror based on folded dual s-shaped bimorphs", *Journal of Microelectromechanical Systems* **19**, pp. 1004–1015 (2009).

[11] M. Nakada, C. Chong, A. Morosawa, K. Isamoto, T. Suzuki, H. Fujita, and H. Toshiyoshi, "Optical coherence tomography by all-optical mems fiber endoscope", *IEICE Electronics Express* **7**, pp. 428–439 (2010).

[12] D. Essex, "Tutorial on optomechanical beam steering mechanisms", Technical report University of Arizona.

[13] J. D. Zook, "Light beam deflector performance: a comparative analysis", *Applied Optics* **13**, pp. 875–887 (1974).

[14] Shoude Chang, Erroll Murdock, Youxin Mao, Costel Flueraru, and John Disano, "Stationary-fiber rotary probe with unobstructed 360° view for optical coherence tomography", *Opt. Lett.* **36**(22), pp. 4392–4394 (2011).

[15] "Bringing image-guided laser surgery to endoscopy".

[16] Simon Henein, *Conception des guidages flexibles*, PPUR presses polytechniques (2001).

[17] L. W. Tsai, *Robot Analysis: The Mechanics of Serial and Parallel Manipulators*, Wiley-Interscience (1999).

[18] N. Andreff, S. Dembele, B. Tamadazte, and S. Z. Hussnain, "Epipolar geometry for vision-guided laser surgery", In *Int. Conf. on Informatics in Control, Automation and Robotics (ICINCO'13)* (2013).

[19] D. Kundrat, A. Schoob, B. Munske, and T. Ortmaier, "Towards an endoscopic device for laser-assisted phonomicrosurgery", In *The Hamlyn Symposium on Medical Robotics* (2013).

[20] A. G. Ponomarenko, R. I. Soloukhin, and V. N. Tishchenko, "Optimization and limiting characteristics of co2 lasers", *Journal of Applied Mechanics and Technical Physics* **16**(5), pp. 774–782 (1975).

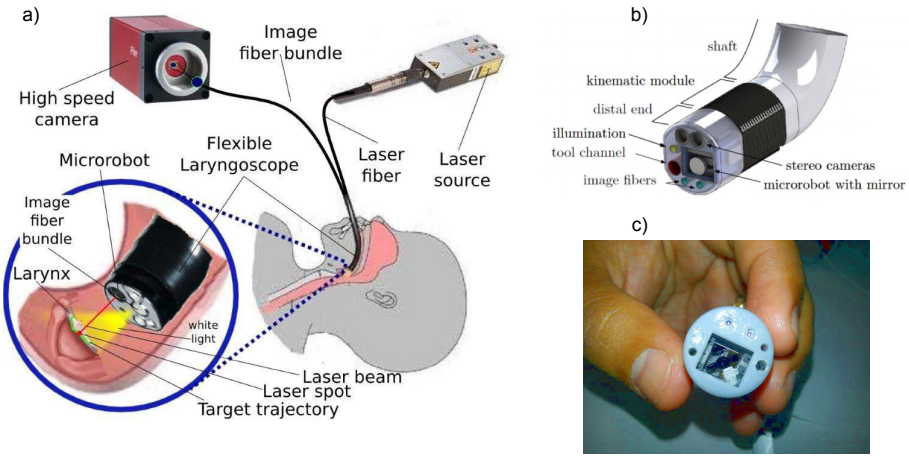

Figure 1: a) A view of the developed concept in μRALP project, b) The endoscope from Liebniz Universitt Hanover [19], and c) Squipabot inside the endoscope tip.

Maximum streering angle	$\pm 15^{\circ}$
Resolution	100 μm
Accuracy	100 μm
Spot size	300 μm
Working distance	40mm
Spectral range	2-11 μm [20]
Throughput	90 %

Table 1: Functional requirements of the beam steering system for laser phonosurgery.

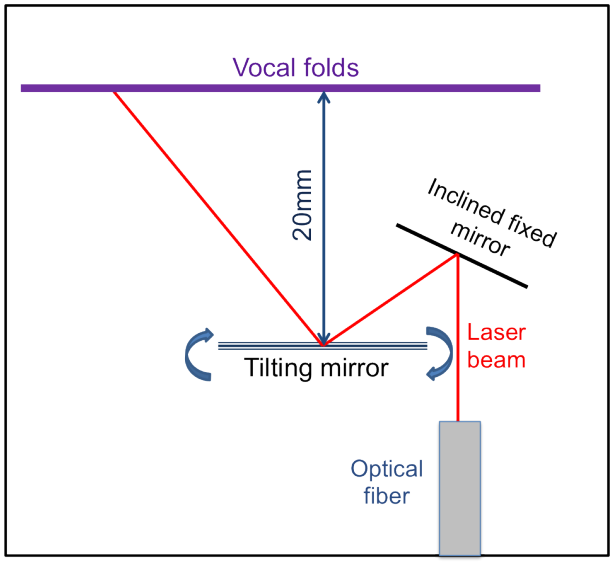

Figure 2: Functioning principle of the steering laser beam robot for phonosurgery.

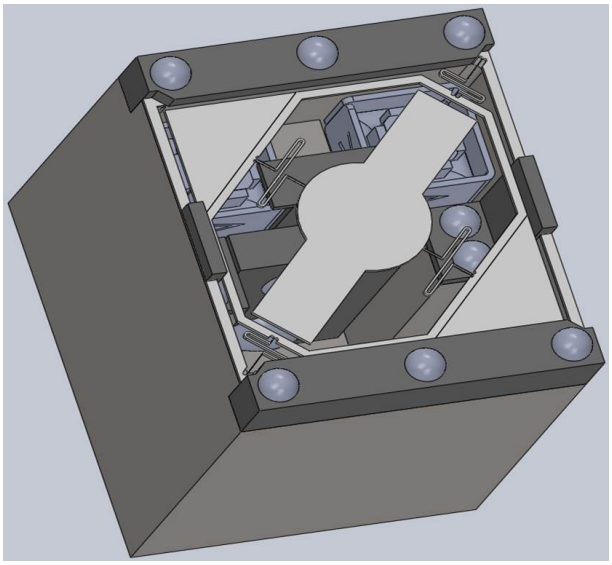

Figure 3: The concept of Squipabot for beam steering with dimension about 8 mm x 10 mm x 12 mm.

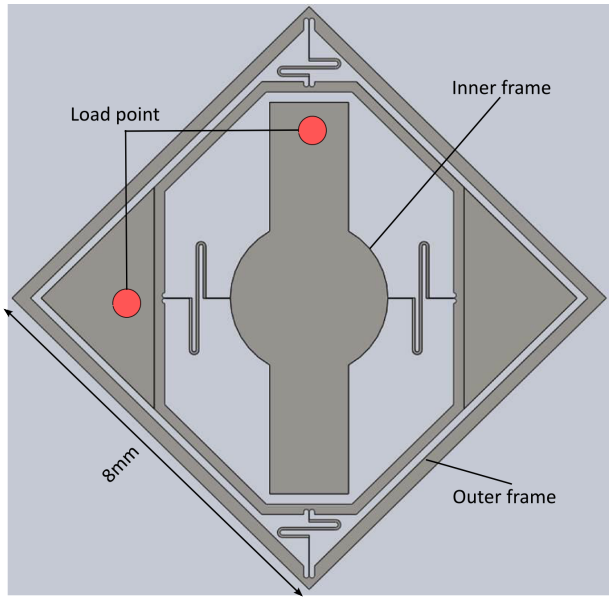

Figure 4: A sketch of the movable platform with inner and outer frame.

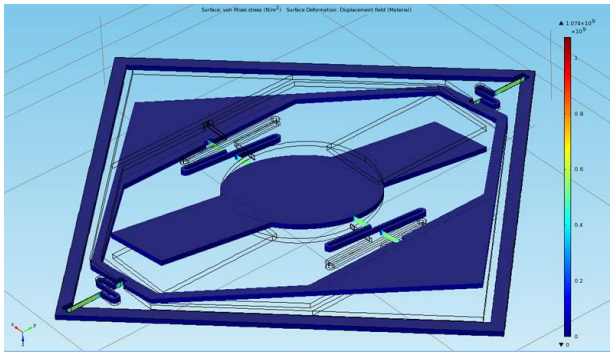

Figure 5: FEM simulation achieved on Comsol® Multiphysics software.

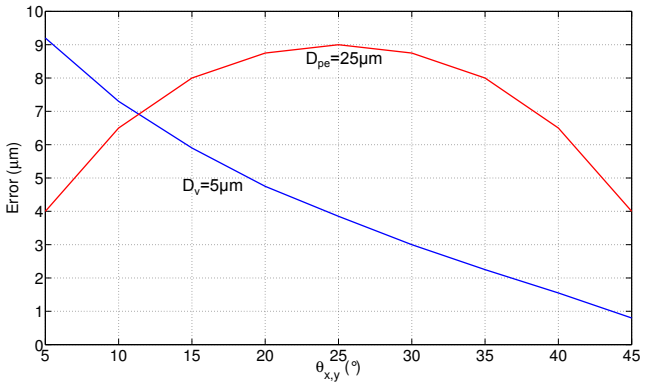

Figure 6: Error on the screen fixed at 20 mm from the mirror center according to steering angle for fixed D_{pe} and D_v.

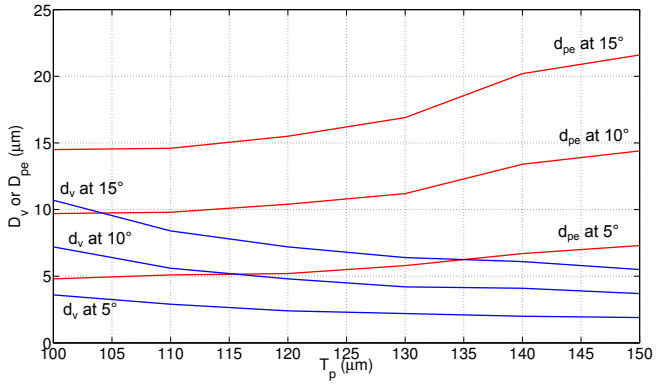

Figure 7: The effect of the platform thickness T_p on D_v and D_{pe}.

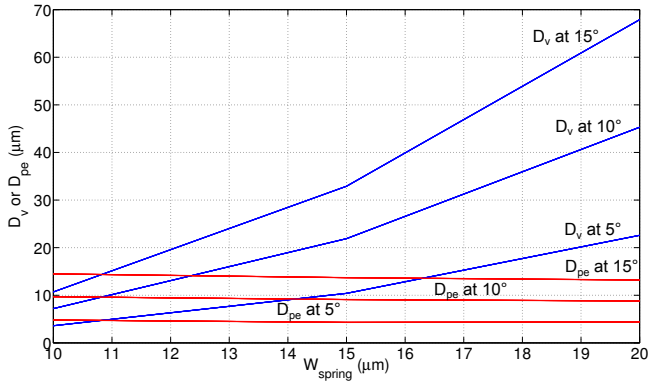

Figure 8: The effect of the spring width on D_{pe} and D_v.

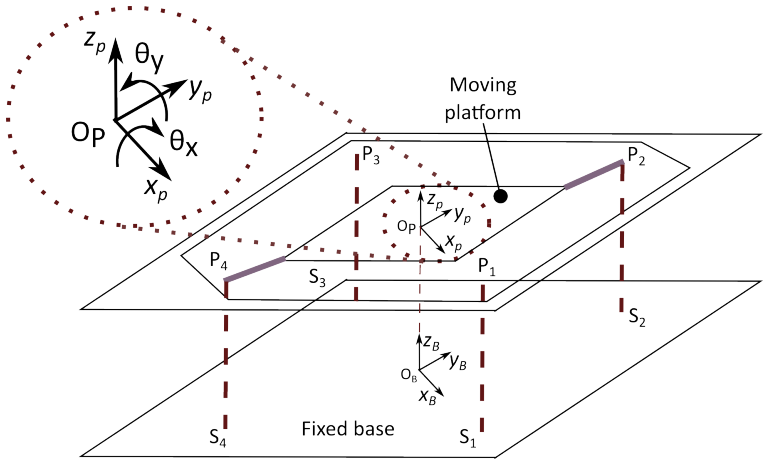

Figure 9: Kinematic model of the parallel mesorobot with four limbs and decoupled two rotations.

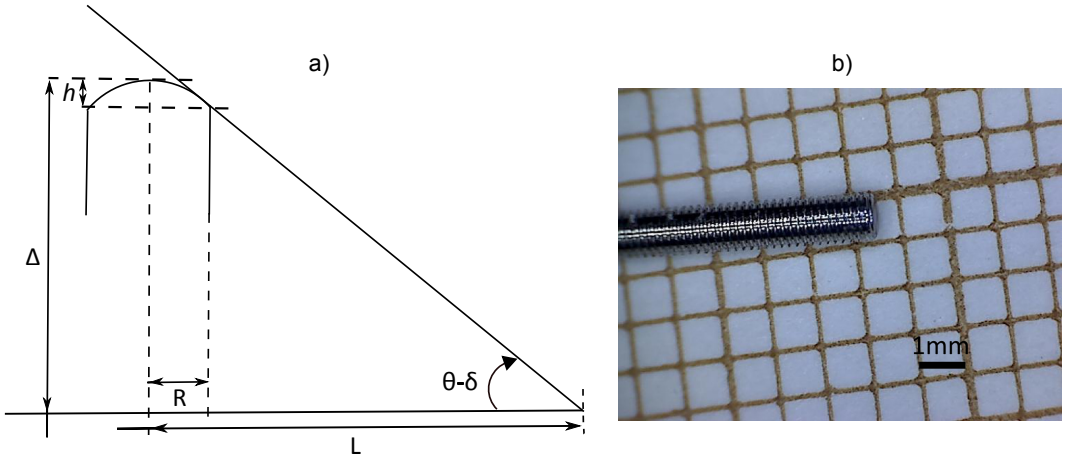

Figure 10: a) Sketch of the contact evolution between the platform and the screw head: L is the distance between the pushing point the center of the mirror, Δ is the displacement of the motor, R is the radius of the screw, h is the height of the cap, θ replaces θ_X or θ_Y, and δ is the deviation angle, and b) the screw head.

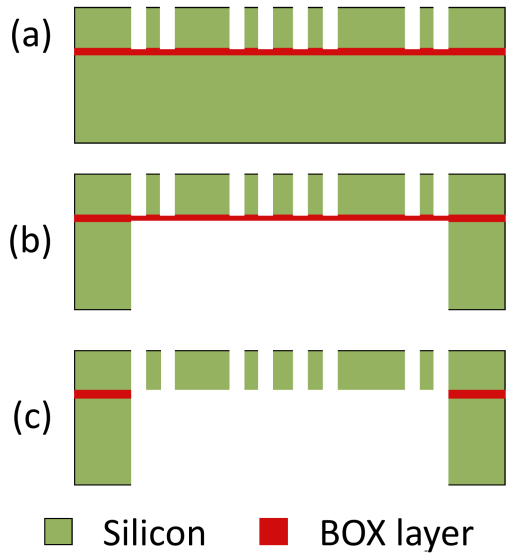

Figure 11: The flowchart of the micromachining: (a) front side DRIE etching, (b) back side DRIE etching , and (c) removal of BOX layer by Freon RIE etching followed by Cr/Au sputtering.

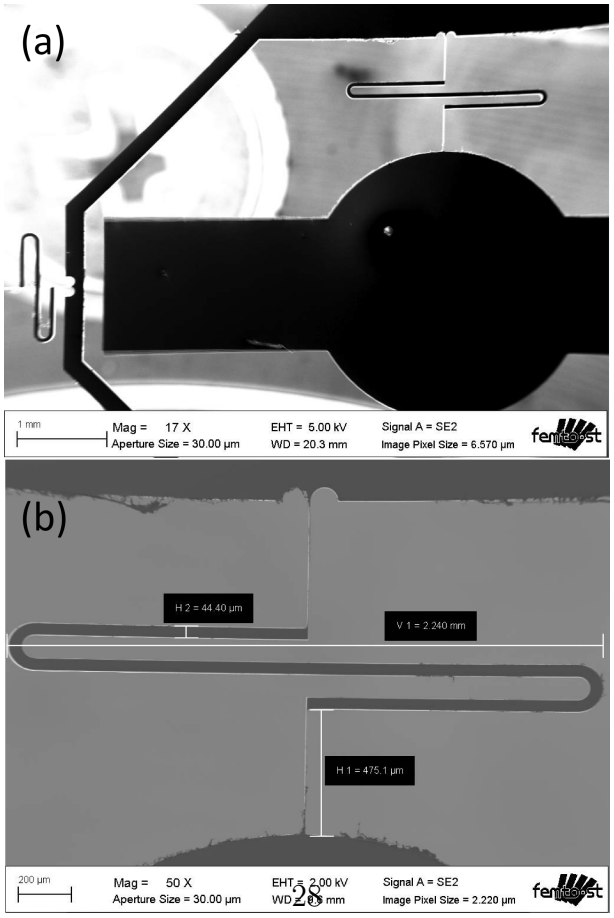

Figure 12: SEM images of the fabricated platform: (a) zoom on the spring, and (b) global view of the platform.

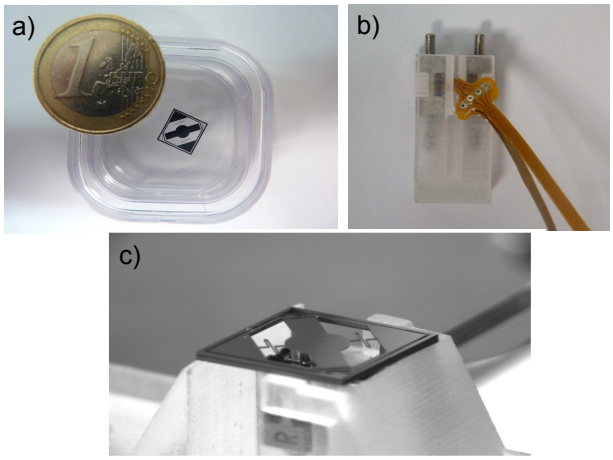

Figure 13: Parts of Squipabot: a) the fabricated platform, b) the actuator unit, and c) the assembly of Squipabot.

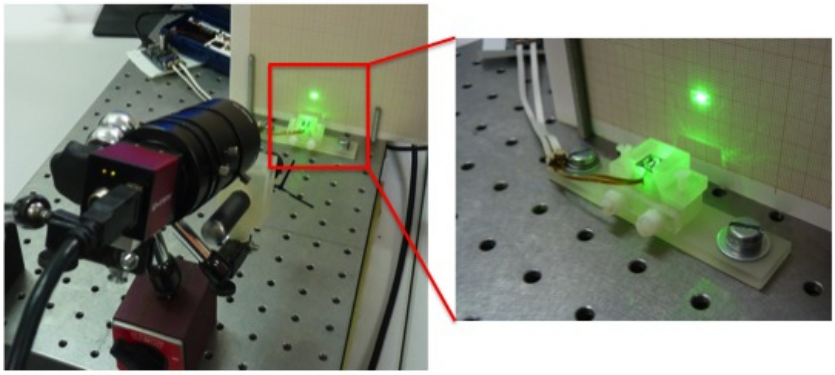

Figure 14: Preliminary tests on the first version of Squipabot with in plane displacement of the spot.

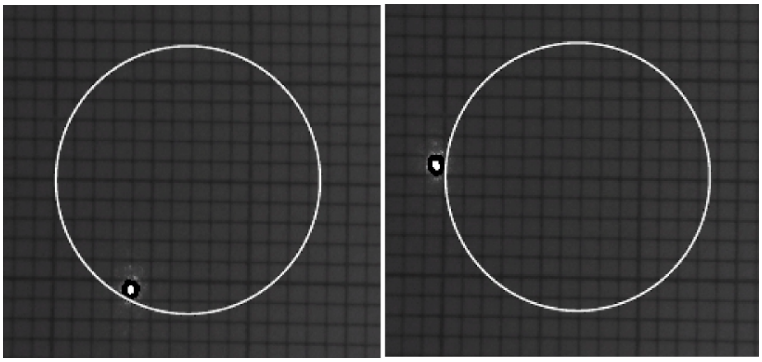

Figure 15: Spot positions on the screen during the test.

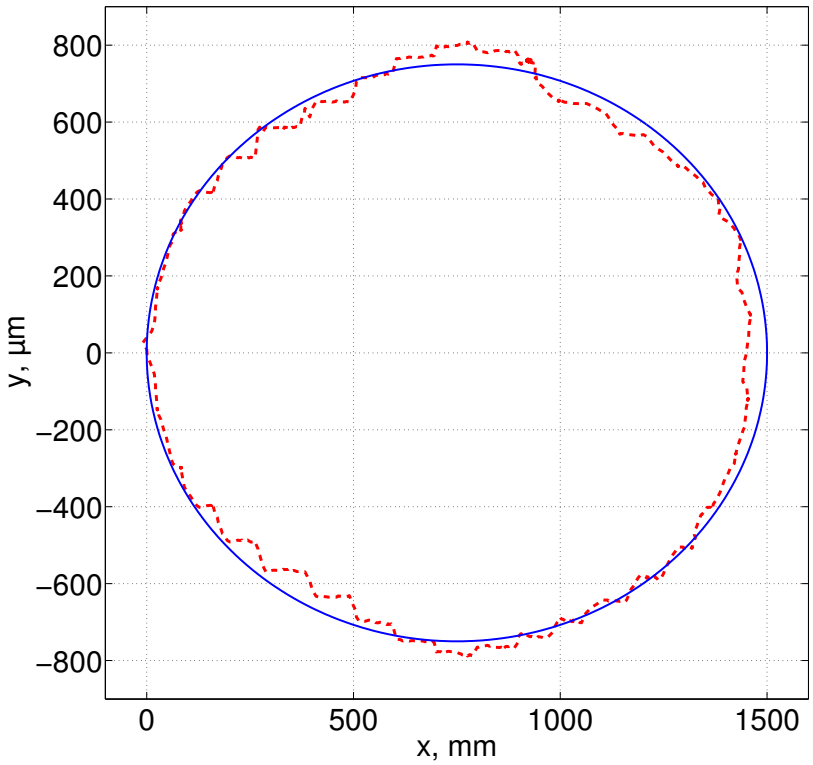

Figure 16: Path following result in open loop control with Squipabot: in red - the reference trajectory and in blue - the achieved trajectory.